https://doi.org/10.3311/PPee.40618
Creative Commons Attribution

Periodica Polytechnica Electrical Engineering and Computer Science

Investigation and Analysis of Electrical Faults in the Seven-phase Induction Machine

Koussaila Iffouzar[1*], Lazhar Roubache [1], Ali Benachour[1]

[1] Laboratoire de Recherche des Systèmes Electrique et de Conversion d'énergie (LRSECE), Département d'Electrotechnique, Ecole Nationale Supérieure des technologies Avancées (ENSTA), P. O. B. 474, 16001 Bab El Oued, Algeria
[*] Corresponding author, e-mail: koussaila.iffouzar@ensta.edu.dz

Received: 04 April 2025, Accepted: 09 September 2025, Published online: 20 October 2025

Abstract

Multiphase induction machines have revolutionized the propulsion and traction sector, thanks to their fault tolerance. This paper is focused on the analysis of electrical faults in the squirrel cage Seven-Phase Induction Machine (SPIM). This study provides a solid basis for diagnosing various faults by analyzing their distinct signatures for the electric faults that can affect this machine. To this end, a transient finite element model is elaborated to study these several electrical faults in SPIM. This paper will be devoted to the study of opening faults in various stator phases (one phase, two adjacent phases, two non-adjacent phases and two far phases), and short-circuiting between turns of stator phases (5%, 10%, 15% of the first phase). An analysis of electromagnetic torque ripple, joule loss and efficiency is undertaken in this paper.

Keywords

multiphase induction machine, finite element method, electrical faults, torque ripples, fault tolerance

1 Introduction

Induction machines are one of the mainstays of modern electromechanical systems. Their robustness, simplicity of design and low maintenance costs make them the preferred choice for a multitude of industrial applications, from motorized drives and pumping systems to electric vehicles, and renewable energies [1–7]. Traditionally, three-phase induction machines have dominated the market due to their technological maturity and compatibility with existing electrical infrastructures. However, changing industrial needs and recent technological advances have highlighted the limitations of these machines, particularly in terms of reliability, performance under variable load and fault tolerance. Multiphase induction machines, particularly those with seven phases, are emerging as a promising alternative [3, 4]. These machines offer significant advantages over their three-phase counterparts, such as a reduction in current harmonics, a better distribution of losses [8–11], and an increased ability to continue operating even in the presence of faults. These characteristics make them particularly suitable for applications where continuity of service is essential [12–17], such as in the transport sectors (land, air, marine and special). However, the complexity of multiphase systems requires an in-depth understanding of their dynamic behavior, particularly under degraded conditions. Faults in induction machines can occur at several levels short-circuits between turns or phases in the stator [14], stator phase opening, and breakage of bars or rings in the rotor, or supply imbalances. These faults can lead to degraded machine performance, increased energy losses, mechanical vibrations and, in the most severe cases, unplanned system shutdowns. Therefore, the behavioral analysis of multiphase induction machines under different types of faults is crucial to ensure their reliability and durability [15–18]. This paper proposes to study in detail the behavior of a seven-phase induction machine subjected to various fault scenarios. The main objective is to understand the impact of these faults on the dynamic performance of the machine, as well as to evaluate its ability to operate in degraded mode. To this end, physical finite element simulations are carried out to analyze the temporal responses of the machine under different fault conditions. The results of this study highlight faults specific to seven-phase induction machines and provide valuable data for the design of diagnostic and fault tolerance strategies. For example, the analysis of current harmonics and electromagnetic torque ripples makes it possible to identify characteristic

Cite this article as: Iffouzar, K., Roubache, L., Benachour A. "Investigation and Analysis of Electrical Faults in the Seven-phase Induction Machine", Periodica Polytechnica Electrical Engineering and Computer Science, 2025. https://doi.org/10.3311/PPee.40618

signatures for each type of fault, paving the way for methods of early detection and dynamic reconfiguration of the system. In addition, the study explores the operational limits of the machine in degraded mode, providing recommendations for optimizing its design and control in critical environments. In short, this research is contributing to a better understanding of seven-phase induction machines. Advances in this field are essential to meet the growing demands of modern electrical systems, where performance, safety and durability are top priorities. This paper is divided into five sections; after a brief introduction, the modeling of the seven-phase induction machine using the finite element method is presented in Section 2. Section 3 deals with the analysis of the various stator phase electrical faults. The results obtained are summarized and interpreted by overview in Section 4, before ending with a conclusion.

2 Modeling of the SPIM using the finite element method

As shown in Fig. 1 the stator windings of the SPIM are shifted by 51.4°. To analyze different performances developed in the studied seven-phase induction machine (SPIM) under healthy and fault operating conditions, a transient finite element model is constructed using Maxwell Electronics software [19]. The model is based on a two-dimensional analysis; therefore, end effects and rotor skew are neglected. Table 1 lists the geometrical and electrical parameters of the machine.

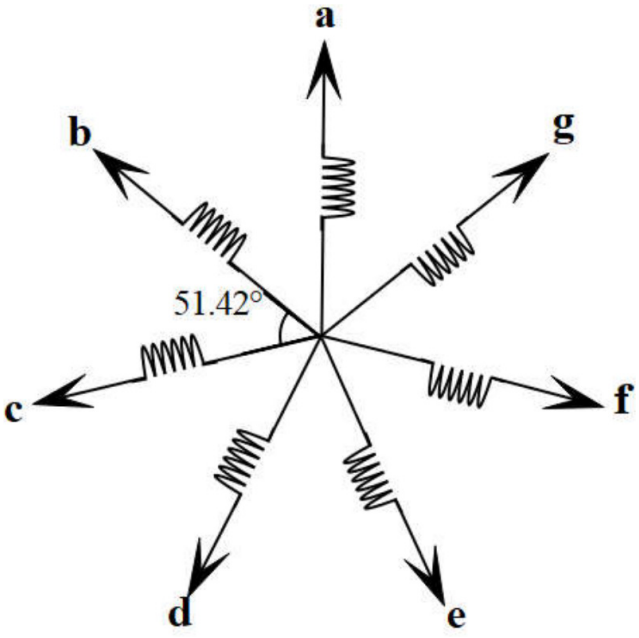

Fig. 1 Spatial repartition of SPIM stator winding

Table 1 Geometric parameter of the SPIM

Parameter	Values
Power	4.5 kW
Rated voltage	160 V
Rated current	4.5 A
Rated speed	1425 rmp
Rated slip	5%
Pole pairs	2
Frequency	50 Hz
Efficiency	94%
Outer stator diameter	110 mm
Inner stator diameter	74 mm
Number of phases	7
Number of stator slots	28
Number of spires per phase	120
Air gap length	0.5 mm
Outer rotor diameter	73.5 mm
Inner rotor diameter	50 mm
Number of rotor bars	38

After defining the geometrical parameters and constructing the 2-D model, the following procedures are applied to adapt the model to the case study presented in this paper:

- *Rotor Motion:* The rotor is set into rotational motion at the rated speed of the machine Ω_r=1425.
- *Stator Winding Distribution:* The stator windings are distributed in the stator slots so that the seven phases are mechanically shifted by an angle of $\frac{2\pi}{7p}$, where p is the number of pole pairs, as shown in Fig. 2.
- *Voltage Supply:* The phase windings are fed by a balanced seven-phase voltage system:

$$\begin{cases} V_1 = \sqrt{2}V_m \sin(\omega t) \\ V_2 = \sqrt{2}V_m \sin\left(\omega t - \frac{2\pi}{7}\right) \\ \quad \ldots \\ V_7 = \sqrt{2}V_m \sin\left(\omega t - \frac{12\pi}{7}\right) \end{cases} . \tag{1}$$

Where V_m is the rated voltage and ω is the angular frequency.

The transient field-circuit coupling is described by Eq. (2):

$$\nabla \times \left(\frac{1}{\mu} \nabla \times A_Z \right) = J_S - \sigma \frac{\partial A_Z}{\partial t} \tag{2}$$

where μ is the magnetic permeability, A_Z is the z-component of the magnetic vector potential, J_S is the stator current density, and σ is the rotor bar conductivity.

The stator current density J_S is derived from the induced stator current, calculated via the circuit equation:

$$V_n = R_S i_n + \frac{\partial \Phi_n}{\partial t} \tag{3}$$

where V_n, R_S, Φ_n, and i_n are the source voltage, source voltage resistance, magnetic flux linkage, and phase current of the n^{th} phase, respectively.

After meshing the study domain (Fig. 2), the transient magnetic field equations are solved iteratively. The torque is computed using the Maxwell stress tensor method. It should be noted that a transient simulation is required to allow rotor currents to reach steady-state values under dynamic conditions.

- *Open-phase Faults:* Open-phase faults in one or two phases are simulated by assigning an infinite source voltage resistance (i.e., $R_S = 1\text{M}\Omega$) to the corresponding phases, thereby enforcing zero current in those phases.
- *Partial Short-circuit Faults:* Partial short-circuit conditions in a phase are simulated by reducing the number of turns in the affected phase while keeping the number of turns constant for the other phases (e.g., for a 5% short-circuit in phase A, the number of turns is reduced to $N_{ph}^{A} = 114$ spires).

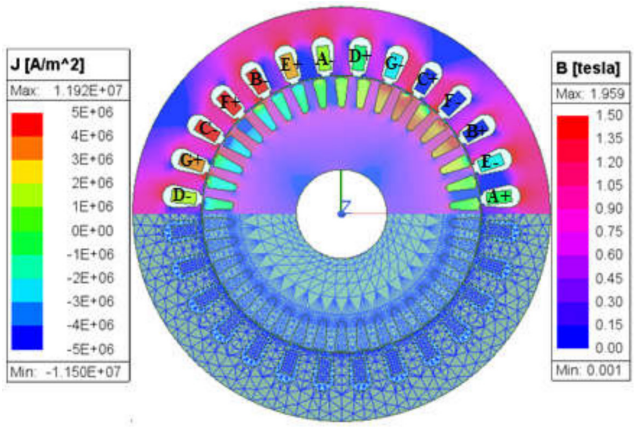

Fig. 2 Flux Density, induced current, and mesh distribution in the healthy condition at rated speed

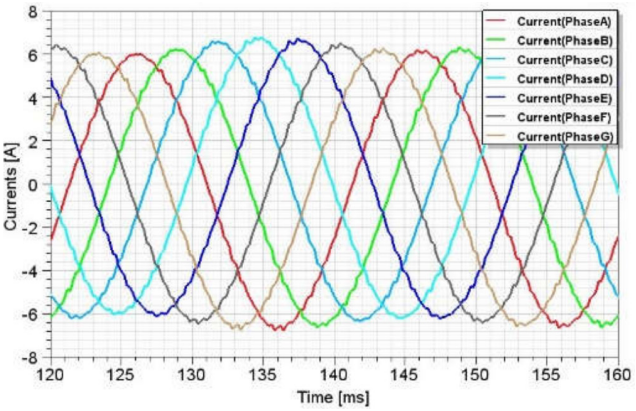

Fig. 3 Stator current of SPIM in healthy condition

Figs. 2–3 show the preliminary results of the SPIM in the healthy state, i.e. the distribution of the magnetic induction, the current density and the temporal evolution of the phase currents.

3 Analysis of electrical phase faults in the stator of SPIM

The seven-phase induction machine offers continuity of service during stator phase faults, something that is not possible with the three-phase machine. This section discusses the various phase faults that can occur in a seven-phase induction machine with nominal torque load ($T_n = 30$ N m) several scenarios have been developed for this purpose.

3.1 Open phase scenarios

Fig. 4 summarizes the different open phase scenarios as like:

- Opening of stator phase A,
- Opening of two stator phases A and B (Adjacent phase),
- Opening of two stator phases A and C (non- adjacent phases),
- Opening of two stator phases A and D (two far phase).

Figs. 5–8 show the stator currents of the SPIM under different stator phase opening faults, with an imbalance in the amplitudes of the currents of the healthy phases. The RMS value of the G phase current I_{gs} is highest when the A phase

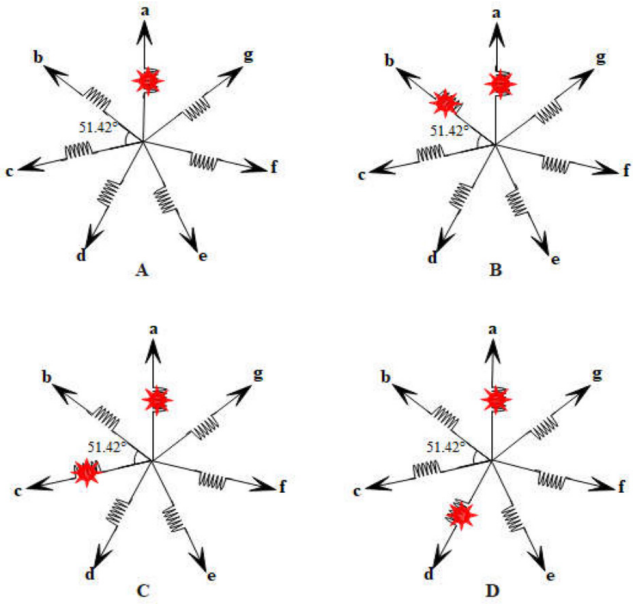

Fig. 4 Different cases of open stator phase in SPIM: (a) phase A – one phase open, (b) phase B – two adjacent phase open, (c) phase C – two non-adjacent phases open, (d) phase D – two far phase open

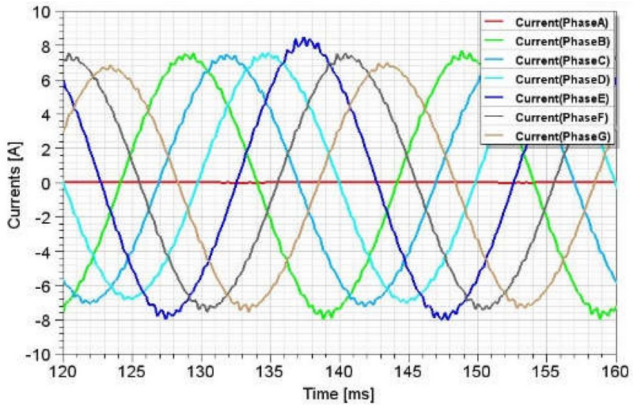

Fig. 5 Stator currents with phase A opened

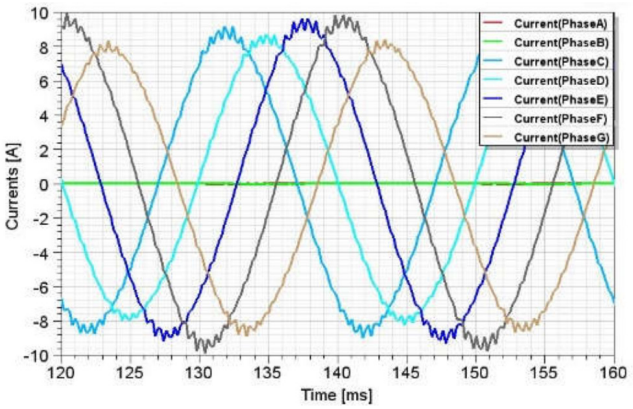

Fig. 6 Stator currents with phase A and B opened

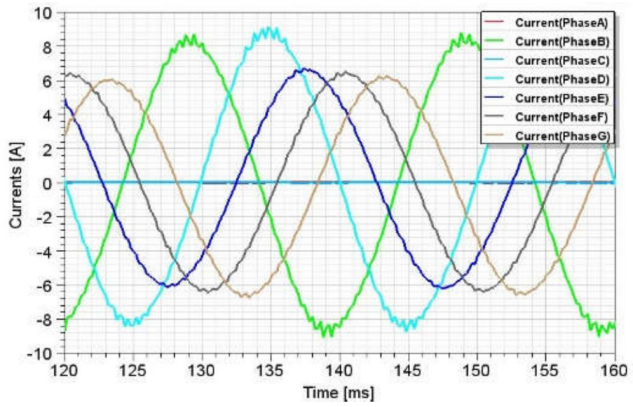

Fig. 7 Stator currents with phase A and C opened

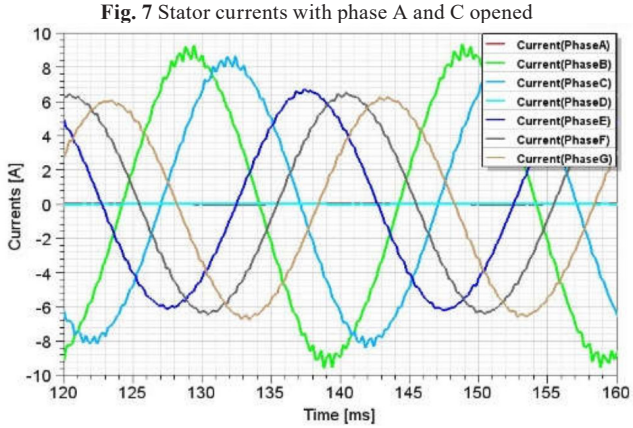

Fig. 8 Stator currents with phase A and D opened

is open. With regard to the opening of two adjacent phases (A and B), Fig. 6 shows that the current of phase F i_{fs} has the greatest amplitude and that i_{gs} has the greatest RMS value. The highest RMS value of current is noted when the two phases A and D are opened at phase B i_{bs}, with an increase of 40% in RMS value compared with normal operation.

Fig. 9 shows the ripples in the electromagnetic torque under the different types of phase opening. The faulty opening of the two phases (A and D) generates the highest value ("peak to peak") with an 85% increase compared with the nominal electromagnetic torque. This leads to significant mechanical vibrations.

3.2 Short-circuit between stator phase windings

Short-circuiting is one of the most dangerous faults the SPIM can suffer. For this purpose, a short circuit between turns (5%, 10%, 15%) of the stator winding A is analyzed as follows.

Figs. 10–12 show the currents during a short circuit between turns of phase A, the currents of the other phases lose their stability when the number of short-circuited turns increases (5%, 10% and 15%), this imbalance

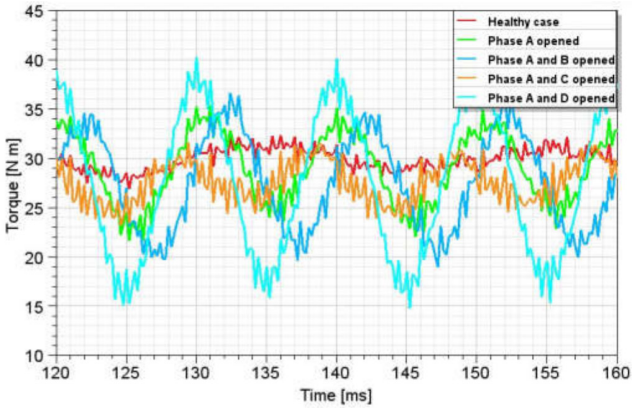

Fig. 9 Electromagnetic torque ripples for healthy and different stator open phase faults

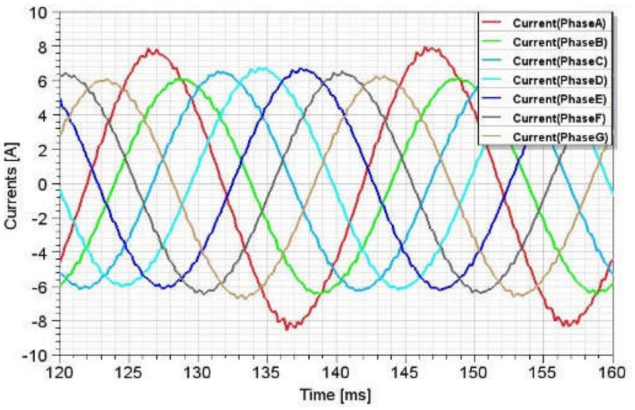

Fig. 10 Stator currents with short-circuit of 5% between turns of phase A

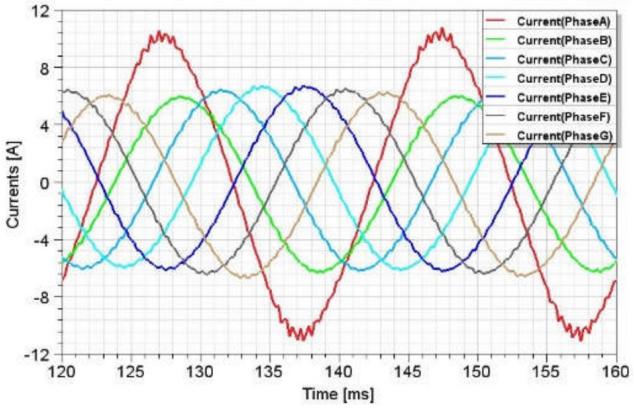

Fig. 11 Stator currents with short-circuit of 10% between turns of phase A

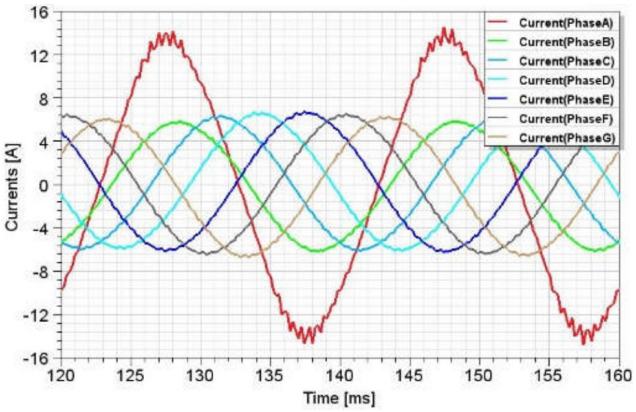

Fig. 12 Stator currents with short-circuit of 15% between turns of phase A

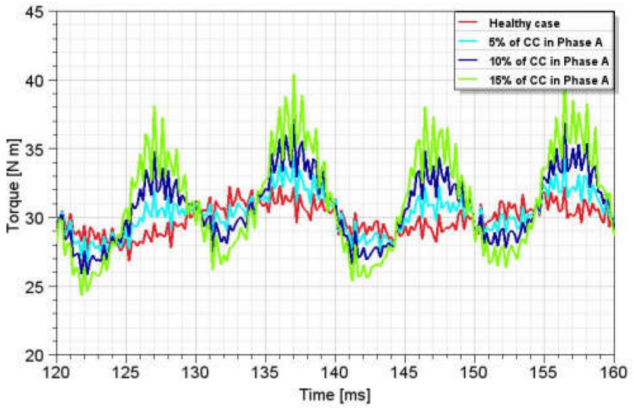

Fig. 13 Electromagnetic torque ripples under several short-circuits between turns of phase A

generates significant electromagnetic torque ripples in the machine, see Fig. 13.

4 Analysis and discussion of results

After processing the results, i.e. calculating the electromagnetic torque ripple ratio

$$\Gamma_{\text{ripples}}(\%) = \frac{\Gamma_{\text{ripples}}(\text{peak to peak})}{\Gamma_{\text{nominal}}} \tag{4}$$

the ratio of stator joule losses

$$P_{\text{Joule}}(\%) = \frac{\sum R_S \times \left(i_{ns}^{rms}\right)^2}{P_{\text{nominal}}} \tag{5}$$

where $n = a,b,...,g$ and s is referred to the stator.
And the efficiency given by the software [19] using:

$$\eta = \frac{P_u}{P_{ab}} \tag{6}$$

where P_u is the useful power and P_{ab} is the absorbed electric power.

The results are summarized in Table 2. All the SPIM electrical fault results are summarized in this section see Figs. 14 and 15. Fig. 15 shows a summary of the electromagnetic torque ripples, the opening fault of two far phases (A and D), generates 85.1% ripple compared with healthy operation, which explains the lower efficiency during this fault **90.85%** see Table 2. It should also be noted that opening phase A generates more ripple than opening phases A and C (two non-adjacent phases), which gives an idea of how to reconfigure the machine when one or more phases

Table 2 Summary of the performance of the seven-phase induction machine under various electrical faults

Case	Torque ripples [%]	Joule losses [%]	Efficiency [%]
Healthy case	18.47	3.87	94.12
Phase A opened	45.73	3.89	92.79
Phase A and B opened	58.9	4.09	90.92
Phase A and C opened	28.8	3.62	90.95
Phase A and D opened	**85.1**	3.65	**90.85**
Short-circuit of Phase A 5%	25.74	4.13	93.97
Short-circuit of Phase A 10%	18.47	4.65	93.51
Short-circuit of Phase A 15%	53.64	**5.62**	92.55

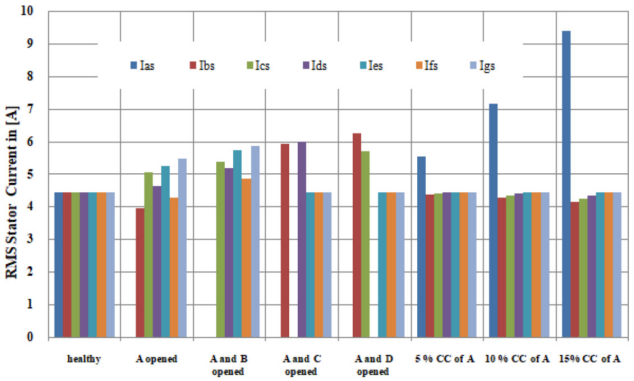

Fig. 14 Summary of the RMS stator currents of the SPIM under various electrical faults

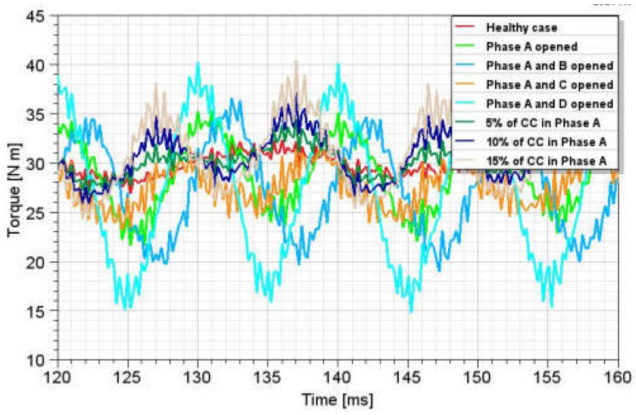

Fig. 15 Electromagnetic torque ripples of all electrical faults

are opened. Phase A is offset by an angle of 102.84° with respect to phase C, so the two phases are almost perpendicular. A reconfiguration for operation at 1/4 of the rated power is conceivable for the opening fault of a single phase with low ripple of the electromagnetic torque. As a perspective, this theory of physical reconfiguration of the machine windings can be envisaged for each type of phase opening fault. Fig. 14 summarizes the RMS value of the stator currents for all the electrical faults. The loss of a phase leads to an unbalance of all the machine currents, unlike the opening of non-adjacent and distant phases. The 15% short-circuit fault causes the machine to overheat, resulting in ripples in the permissible torque (see Table 2).

5 Conclusion

Several electrical faults in the stator of the SPIM have been studied and analyzed in this work. Stator phase opening has a serious impact on efficiency and electromagnetic torque ripples. The opening fault of the two distant phases is classified as the most harmful for the SPIM. A theory for the physical reconfiguration of the SPIM has clearly emerged. When one phase fails to open, it is advisable to open the phase not adjacent to it, as the angle separating them is close to 90°. And for operation with acceptable torque ripples, it is advisable to reduce the power demand by 1/4. This theory can be extended to all SPIM phase opening faults, which will enable a complete SPIM reconfiguration strategy to be developed. Short-circuit faults are shown to be particularly destructive, with fault currents in the affected winding increasing significantly (as seen in the analysis), posing a severe thermal risk and requiring fast-acting protection.

References

[1] Bao, F., Yang, S., Xie, Z., Zhang, X. "A machine interface for renewable energy integration: dual winding induction machine-based generating system", Electrical Engineering, 107(8), pp. 9971–9986, 2025.
https://doi.org/10.1007/s00202-025-03010-0

[2] Sapmaz, T., Oner, Y. "A novel hybrid model of electromagnetic performance for induction machine", Electrical Engineering, 104(5), pp. 3381–3390, 2022.
https://doi.org/10.1007/s00202-022-01549-w

[3] Iffouzar, K., Amrouche, B., Otmane Cherif, T., Benkhoris, M.-F., Aouzellag, D., Ghedamsi, K. "Improved direct field oriented control of multiphase induction motor used in hybrid electric vehicle application", International Journal of Hydrogen Energy, 42(30), pp. 19296–19308, 2017.
https://doi.org/10.1016/j.ijhydene.2017.06.195

[4] Amrouche, B., Otmane Cherif, T., Ghanes, M., Iffouzar, K. "A passivity-based controller for coordination of converters in a fuel cell system used in hybrid electric vehicle propelled by two seven phase induction motor", International Journal of Hydrogen Energy, 42(42), pp. 26362–26376, 2017.
https://doi.org/10.1016/j.ijhydene.2017.08.099

[5] Barrero, F., Duran, M. J. "Recent Advances in the Design, Modeling, and Control of Multiphase Machines–Part I", IEEE Transactions on Industrial Electronics, 63(1), pp. 449–458, 2016.
https://doi.org/10.1109/TIE.2015.2447733

[6] Malathy, N., Sukhi, Y. "Improved start-up strategy for a doubly fed induction machine fed large rated variable speed pumped storage unit in pumping mode operation", Electrical Engineering, 106(1), pp. 615–629, 2024.
https://doi.org/10.1007/s00202-023-02007-x

[7] Kong, W., Kang, M., Li, D., Qu, R., Jiang, D., Gan, C. "Investigation of Spatial Harmonic Magnetic Field Coupling Effect on Torque Ripple for Multiphase Induction Motor Under Open Fault Condition", IEEE Transactions on Power Electronics, 33(7), pp. 6060–6071, 2018.
https://doi.org/10.1109/TPEL.2017.2737027

[8] Cheaytani, J., Benabou, A., Tounzi, A. Dessoude, M. "Stray Load Losses Analysis of Cage Induction Motor Using 3-D Finite-Element Method with External Circuit Coupling", IEEE Transactions on Magnetics, 53(6), 8202104, 2017.
https://doi.org/10.1109/TMAG.2017.2661878

[9] Xue, S., Feng, J., Guo, S., Chen, Z., Peng, J., Chu, W. Q., Xu, P. L., Zhu, Z. Q. "Iron Loss Model for Electrical Machine Fed by Low Switching Frequency Inverter", IEEE Transactions on Magnetics, 53(11), 2801004, 2017.
https://doi.org/10.1109/TMAG.2017.2696360

[10] Jia, H., Yang, J., Deng, R., Wang, Y. "Loss Investigation for Multiphase Induction Machine under Open-Circuit Fault Using Field–Circuit Coupling Finite Element Method", Energies, 14(18), 5686, 2021.
https://doi.org/10.3390/en14185686

[11] Tani, A., Mengoni, M., Zarri, L., Serra, G., Casadei, D. "Control of Multiphase Induction Motors with an Odd Number of Phases Under Open-Circuit Phase Faults", IEEE Transactions on Power Electronics, 27(2), pp. 565–577, 2012.
https://doi.org/10.1109/TPEL.2011.2140334

[12] Bermudez, M., Gonzalez-Prieto, I., Barrero, F., Guzman, H., Kestelyn, X., Duran, M. J. "An Experimental Assessment of Open-Phase Fault-Tolerant Virtual-Vector-Based Direct Torque Control in Five-Phase Induction Motor Drives", IEEE Transactions on Power Electronics, 33(3), pp. 2774–2784, 2018.
https://doi.org/10.1109/TPEL.2017.2711531

[13] Amirouche, E., Iffouzar, K., Houari, A., Ghedamsi, K., Aouzellag, D. "Behavior analysis of dual-star permanent magnet synchronous generator with inter-turn short fault", International Journal of Modelling and Simulation, 2024.
https://doi.org/10.1080/02286203.2023.2299898

[14] Fu, J.-R., Lipo, T. A. "Disturbance-free operation of a multi-phase current-regulated motor drive with an opened phase", IEEE Transactions on Industry Applications, 30(5), pp. 1267–1274, 1994.
https://doi.org/10.1109/28.315238

[15] Duran, M. J., Gonzalez-Prieto, I., Rios-Garcia, N., Barrero, F. "A Simple, Fast, and Robust Open-Phase Fault Detection Technique for Six-Phase Induction Motor Drives", IEEE Transactions on Power Electronics, 33(1), pp. 547–557, 2018.
https://doi.org/10.1109/TPEL.2017.2670924

[16] Huangfu, Y., Wang, S., Qiu, J., Zhang, H., Wang, G., Zhu, J. "Transient Performance Analysis of Induction Motor Using Field-Circuit Coupled Finite-Element Method", IEEE Transactions on Magnetics, 50(2), pp. 873–876, 2014.
https://doi.org/10.1109/TMAG.2013.2281314

[17] Dlala, E., Bottauscio, O., Chiampi, M., Zucca, M., Belahcen, A., Arkkio, A. "Numerical Investigation of the Effects of Loading and Slot Harmonics on the Core Losses of Induction Machines", IEEE Transactions on Magnetics, 48(2), pp. 1063–1066, 2012.
https://doi.org/10.1109/TMAG.2011.2172577

[18] Fratila, M., Benabou, A., Tounzi, A., Dessoude, M. "Calculation of Iron Losses in Solid Rotor Induction Machine Using FEM", IEEE Transactions on Magnetics, 50(2), pp. 825–828, 2014.
https://doi.org/10.1109/TMAG.2013.2281492

[19] ANSYS "Ansys Maxwell, 2024 R1" [computer program] Available at: https://www.ansys.com/products/electronics/ansys-maxwell [Accessed: 18 February 2025]